Supporting Information

A multistage pathway for human prion protein aggregation in vitro: from multimeric seeds to β-oligomers and non-fibrillar structures

Kang R. Cho[†,‡], Yu Huang[*,‡], Shuiliang Yu[§], Shaoman Yin[§], Marco Plomp[†], S. Roger Qiu[†], Rajamani Lakshminarayanan[¶,⌜], Janet Moradian-Oldak[¶], Man-Sun Sy[§], and James J. De Yoreo[*,†,#]

[†]Physical and Life Sciences Directorate, Lawrence Livermore National Laboratory, Livermore, CA 94551, USA; [‡]Department of Materials Science and Engineering, University of California, Los Angeles, Los Angeles, CA 90095, USA; [§]Department of Pathology, Case Western Reserve University, Cleveland, OH 44120, USA; [¶]Center for Craniofacial Molecular Biology, School of Dentistry, University of Southern California, CA 90033, USA; [#]Molecular Foundry, Lawrence Berkeley National Laboratory, Berkeley, CA 94720, USA. [⌜]Present address: Singapore Eye Research Institute, 7 Hospital Drive, Block C, 02-02, Singapore 169611.
[*]To whom correspondence should be addressed: jjdeyoreo@lbl.gov, yhuang@seas.ucla.edu

The Supporting Information Contains:

1. Figure S1……..S2
2. Figure S2……..S4
3. Figure S3……..S7
4. Figure S4……..S8
5. Figure S5……..S10
6. Figure S6……..S13
7. Figure S7……..S16
8. Figure S8……..S19
9. Figure S9……..S23
10. Figure S10……..S26
11. References……..S28

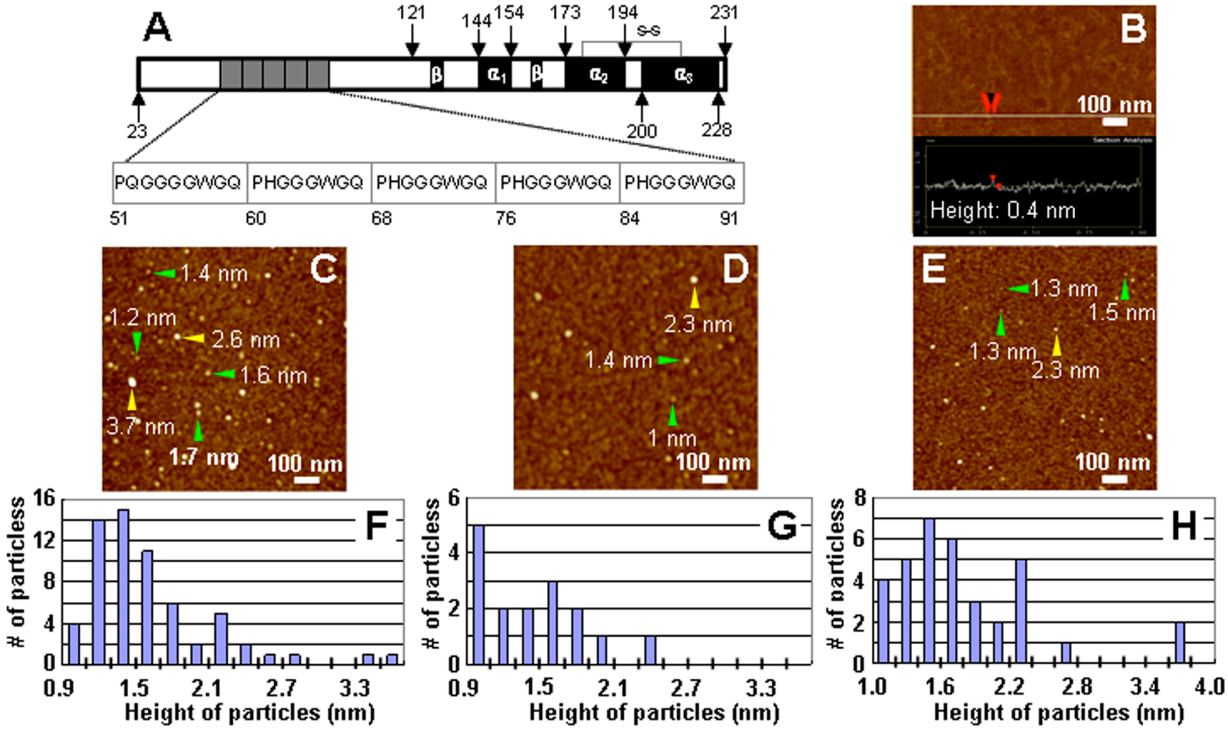

Figure S1. Primary structure, AFM images, and heights of the recombinant human prion proteins. (A) Location and extent of octapeptide repeat region in wild type rPrP^{C} (WT) (drawn taking ref 1). Insertion mutants have variation in number of octapeptide (PHGGGWGQ) repeats, compared to the WT with five octapeptide repeats. (B-E) *Ex situ* AFM images of buffer solution, WT and 10OR: (B) Buffer (20 mM NaOAc (pH 5.5)) image for control. Maximum roughness was approximately 0.4 nm (height: 0.4 nm); (C) WT and (D, E) 10OR in 20 mM NaOAc (pH 5.5). The rPrP^{C} concentrations for WT and 10OR were 20 μM. Numbers next to arrowheads in (C-E) are the heights of adjacent particles obtained by section analysis of the AFM images. Particles indicated by green arrowheads were considered as monomers of rPrP^{C} and particles by

yellow arrowheads as oligomers based on the calibration curve in Figure 2 in the paper.

Due to the effect of AFM tip convolution, a presumed monomer with a height of 1.7 nm in (C) has an apparent diameter of about 20 nm, which is much larger than its hydrodynamic diameter of 4.8 nm.[2] 10OR particles in (E) appear to have similar heights to those in (D), but have smaller diameters. This is because the radius of the tip used to collect image (E) was smaller than that used for image (D). Although tips of the brand (type: FM) were used for all imaging, they had varying tip radii (approximately 5-10 nm) and became blunt during continuous imaging. This small difference in tip size was sufficient to make identical particles on the order of $rPrP^C$ monomers and small oligomers appear to have different diameters.

(F, G, H) Height distributions of all the particles seen in the corresponding images (C, D, E), respectively. Taking particles with heights between 0.9 and 2.1 nm as representing monomers in the graphs (F) and (G), the presumed monomer of WT has a height of 1.4 ± 0.25 nm for (F) and the presumed monomer of 10OR has a height of 1.4 ± 0.33 nm for (G). Taking particles of heights between 1.0 and 2.0 nm as representing monomers in the graph (H), the presumed monomer of 10OR has a height of 1.5 ± 0.25 nm (Also see Figure 1, B and F in the paper).

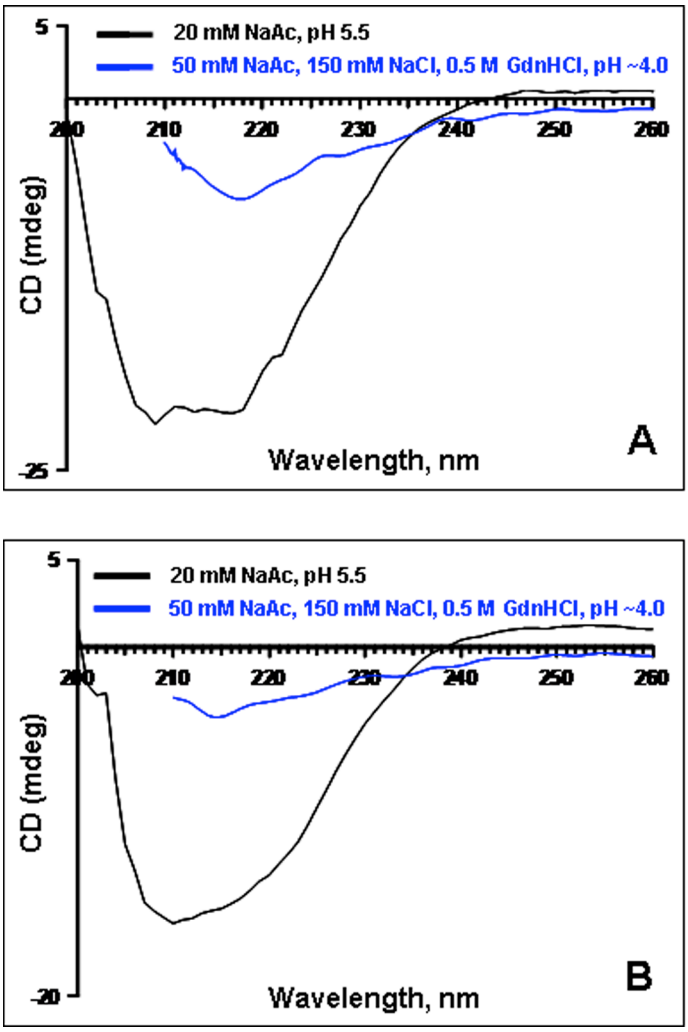

Figure S2. Far ultraviolet (UV) circular dichroism (CD) spectra.

(A) Far UV-CD spectrum of WT in 20 mM NaOAc at pH 5.5 (black line) and in 50 mM NaOAc, 150 mM NaCl, 0.5 M (final concentration) GdnHCl at pH ~4.0 (blue line). At pH 5.5, the presence of double minima at 208 and 222 nm indicates α-helix rich protein. At pH ~4.0, in the presence of 0.5 M GdnHCl, the α-helix rich structure transforms into predominantly β-sheet rich structured conformation, as inferred from the single minimum at 217 nm. (B) Far UV-CD

spectrum of 10OR in 20 mM NaOAc at pH 5.5 (black line) and in 50 mM NaOAc, 150 mM NaCl and 0.5 M (final concentration) GdnHCl at pH ~4.0 (blue line). At pH 5.5, the presence of minima at 208 and a weak shoulder around 222 nm indicates α-helix rich conformation. The weak shoulder around 222 nm may suggest that there is a minor difference between the structure of 10OR and WT, but the overall structure remains almost unaffected by the insertions of octapeptide (PHGGGWGQ) repeats in 20 mM NaOAc, pH 5.5. (In general the minor or negligible change in the structure of pathogenic mutants associated with neurodegenerative diseases, such as the prion protein mutants of this study and amyloid beta (Aβ) peptides, have no tangible effect on their stability in native solution conditions.[3,4]) At pH ~4.0, in the presence of 0.5 M (final concentration) GdnHCl, a minimum around 214 nm indicates the transformation to β-sheet rich structure.

CD spectra were recorded on a Jasco J-810 spectropolarimeter. All the measurements were carried out at 37 °C with 0.1-cm path length sealed cuvette. The instrument optics was flushed with flowing nitrogen at 30 L/min. The instrument settings used were as follows: step resolution 0.2 nm, scan speed 50 nm/min, and bandwidth 2 nm. For each sample, a total of 6 scans were recorded, averaged, and background subtracted. To get CD spectrum of WT and 10OR in 20 mM NaOAc at pH 5.5, 100 µl of 100 µM protein solution (WT or 10OR) in 20 mM NaOAc (pH 5.5) was mixed with 400 µl of the same buffer. 250 µl of this solution containing

final protein concentration of 20 μM was used for the CD measurements. To get CD spectrum of WT and 10OR in 50 mM NaOAc, 150 mM NaCl, 0.5 M (final concentration) GdnHCl at pH ~4.0, first 150 μl of 50 mM NaOAc, 150 mM NaCl (pH 4.0) was added to 100 μl of the protein solution (100 μM) in 20 mM NaOAc (pH 5.5) and mixed thoroughly. To 125 μl of this solution, 125 μl of 50 mM NaOAc, 150 mM NaCl and 1 M GdnHCl (pH 4) was added so as to maintain the final protein concentration 20 μM and GdnHCl 0.5 M at pH ~4.0. The solution was stirred in an incubator at 37 °C for 10 minutes and then, CD spectrum was recorded immediately.

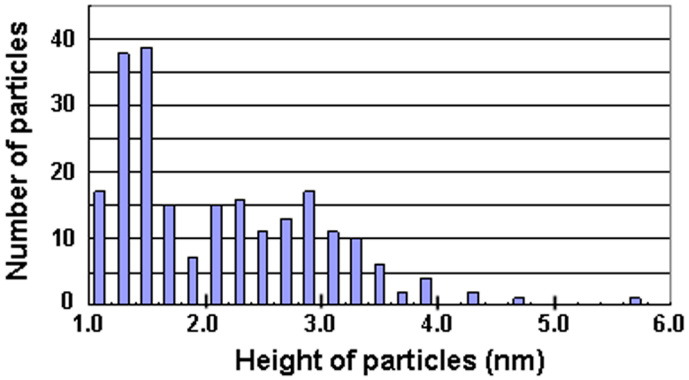

Figure S3. The complete height distribution of 10OR including monomers at t = 0^+ min under *ex situ* conditions.

Heights of particles were measured in two 500 × 500 nm images. One of them is shown as Figure 1D in the paper. It shows that upon partial denaturation, the population immediately transforms from nearly 100 % monomers to a clear bimodal distribution consisting of monomers and trimers/tetramers.

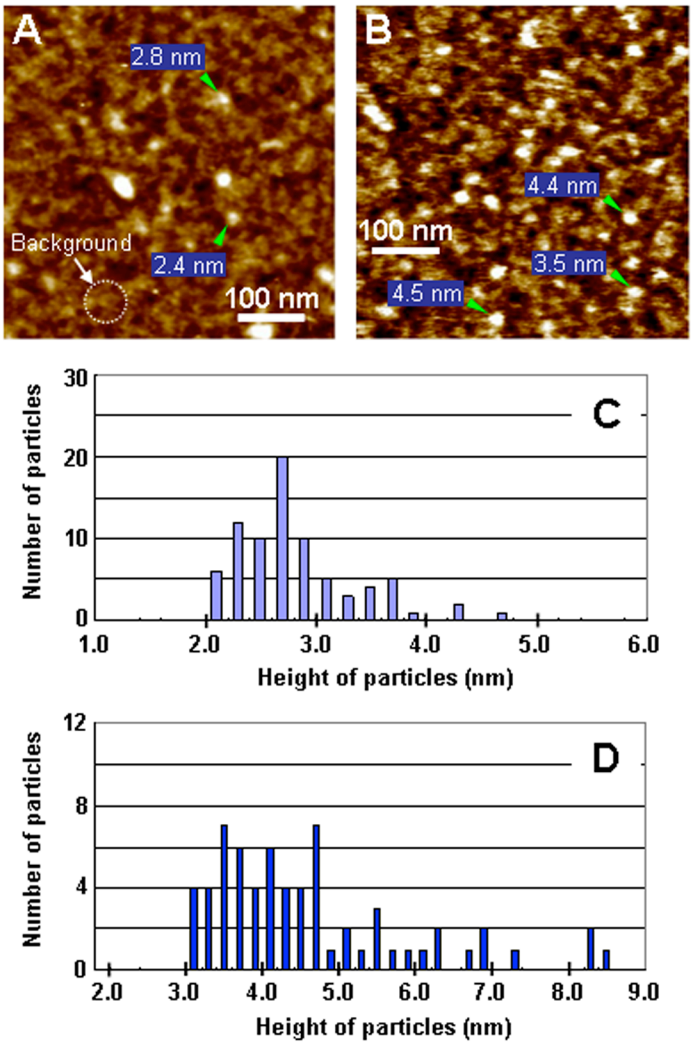

Figure S4. AFM images of bovine serum albumin (BSA) (MW: ~66 KDa) and height distributions.

(A) Height image in air and (B) height image in solution. Particles indicated by green arrowheads in (A) and (B) were presumed to be BSA monomers. (C) The height distribution of BSA particles based on measurements from eight 500×500 nm air images. Particles, with heights between 2.0 and 3.2 nm, were used to estimate the average height of BSA monomers. The

average height obtained this way is 2.6 ± 0.28 nm. (D) The height distribution of BSA particles based on measurements from four 500×500 nm solution images. Particles, with heights between 3.0 and 4.8 nm, were used to estimate the average height of BSA monomers. The average height obtained this way is 4.1 ± 0.67 nm.

To obtain these images, 5 mg of BSA was dissolved in 500 µl of Milli-Q water to produce 1% (w (weight of BSA) /v (volume of water)) solution with pH ~5.2, in which BSA remains primarily in a monomeric state. To get the air image (A), a 10 µl aliquot was deposited on freshly cleaved mica for 4 minutes, rinsed with Milli-Q water and dried with compressed nitrogen gas. The sample was then imaged with tapping mode AFM. To get the solution image (B), 45 µl aliquot was deposited on fleshly cleaved mica secured to the AFM scanner (mica was glued onto round plastic cover slip which was glued to AFM specimen disc (diameter: 15 mm)) and a fluid cell was installed. *In situ* imaging in taping mode was then carried out.

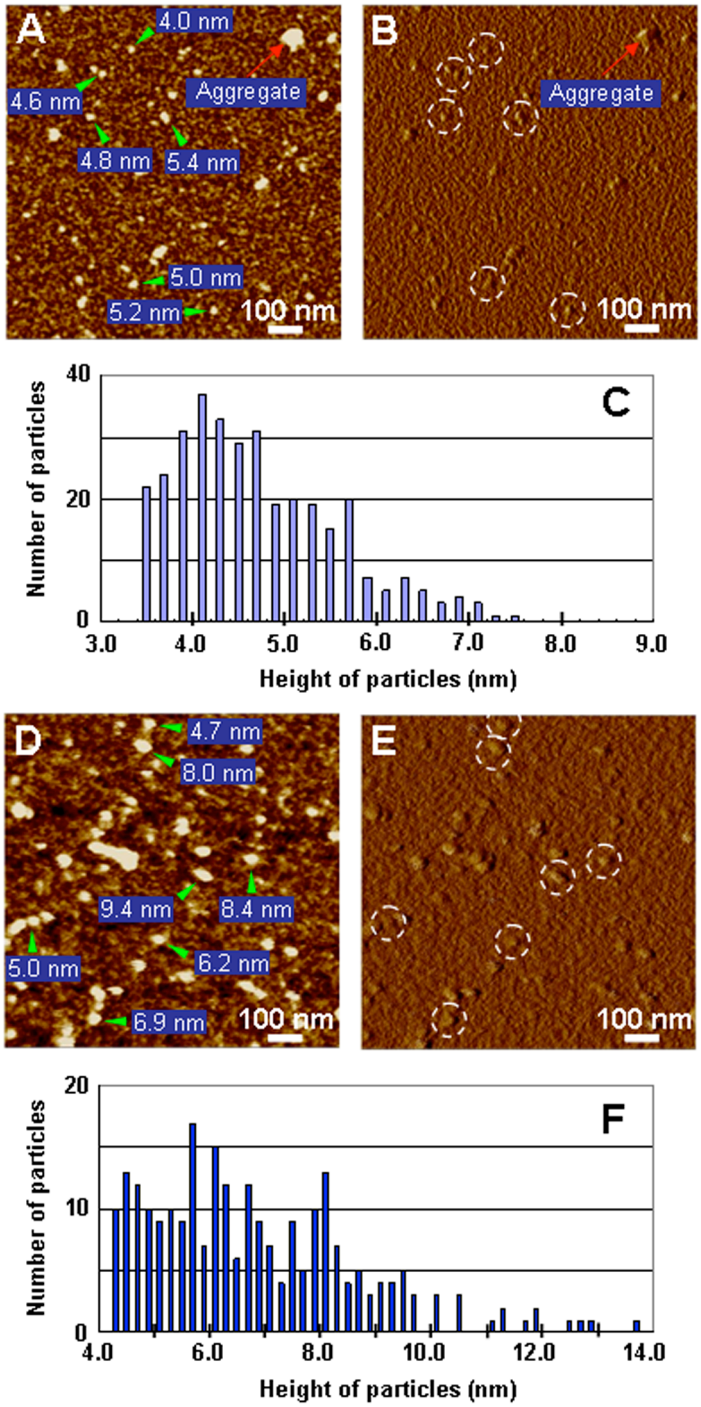

Figure S5. AFM images of Immunoglobulin G from human serum (MW: ~150 KDa) and height distributions.

(A) Height and (B) amplitude images in air. Some Immunoglobulin G particles are indicated by green arrowheads and a red arrow in (A). (C) The height distribution of Immunoglobulin G particles based on measurements from ten 1×1 μm air images. Particles, with heights between 3.4 and 6.0 nm, were taken to be Immunoglobulin G monomers by carefully observing shape in amplitude images. Larger particles appear to be aggregates. The average height of Immunoglobulin G monomers in air images obtained this way is 4.5 ± 0.64 nm. A small number of particles (aggregates) such as one indicated by the red arrow in (A), with height larger than 9 nm were also observed, but they were not included in the graph. (D) Height and (E) amplitude images in solution. Some Immunoglobulin G particles are indicated by green arrowheads in (D). (F) The height distribution in solution, based on measurements from seven 1×1 μm solution images. Particles with heights between 4.2 and 9.6 nm, were used to obtain the average height of Immunoglobulin G monomers on mica in solution. However, careful examination of particle shape suggests that particles with heights between ~9 and 9.6 nm might be actually oligomers. The average height of Immunoglobulin G monomers in solution images obtained this way is 6.2 ± 1.47 nm.

To obtain these images, 5 mg of Immunoglobulin G (MW: ~150 KDa) from human serum (Sigma-Aldrich, 56834-25MG) was dissolved in 500 μl of 20 mM NaOAc, pH 5.5. Then 16 μl of the solution was diluted in the 484 μl of 20 mM NaOAc, pH 5.5 to get ~2.1 μM

Immunoglobulin G solution. To get the air images (A and B), a 10 µl aliquot was deposited on freshly cleaved mica for 4 minutes, rinsed with Milli-Q water and dried with compressed nitrogen gas. The sample was then imaged with tapping mode AFM. To get the solution images (D and E), 45 µl aliquot was deposited on fleshly cleaved mica (diameter: 3 mm) secured to the AFM scanner and a fluid cell was installed. *In situ* imaging in taping mode was then carried out.

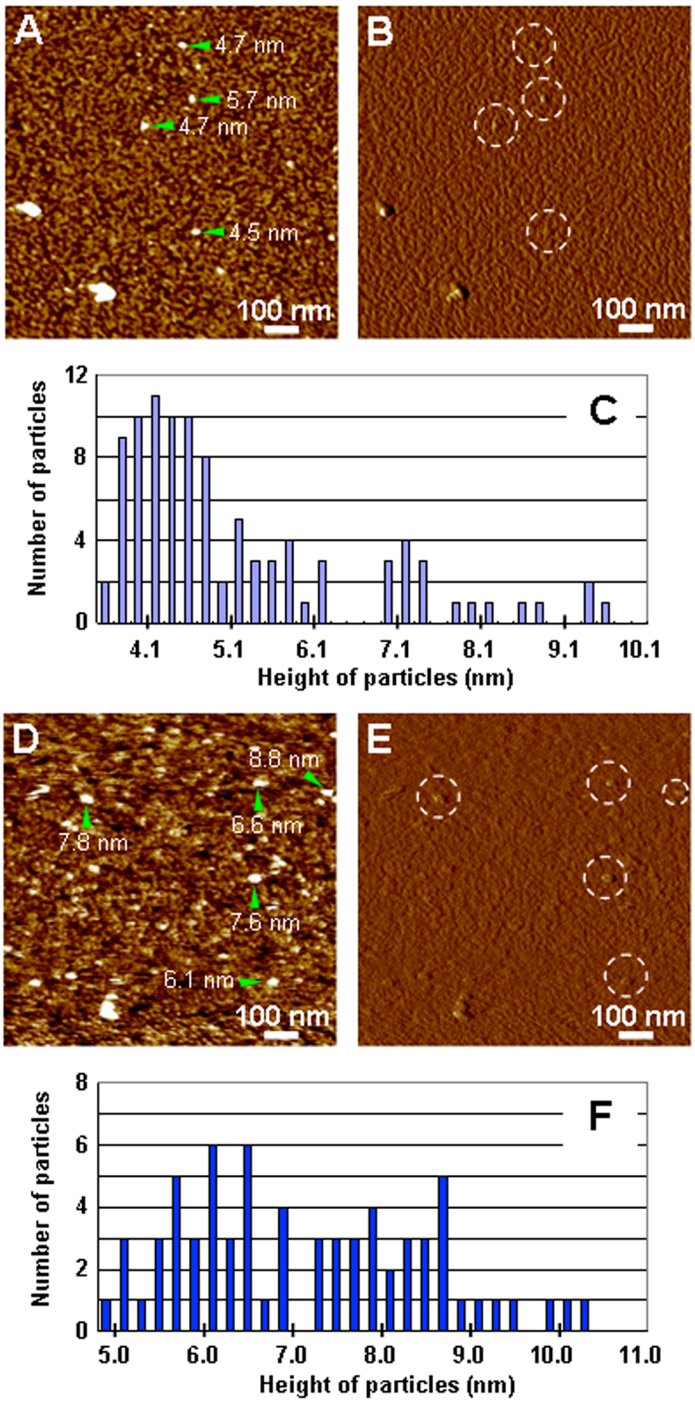

Figure S6. AFM images of mycocerosic acid synthase (MAS) (MW: ~224 KDa) and height distributions.

(A) Height and (B) amplitude images in air. Particles indicated by green arrowheads in (A) were presumed to be MAS monomers. (C) The height distribution of MAS particles based on measurements from ten 1×1 μm air images. Particles, with heights between 3.5 and 5.9 nm, were used to estimate the average height of MAS monomers. The average height obtained this way is 4.5 ± 0.58 nm. A small number of particles with heights larger than 10.1 nm were also observed in the air, but they were not included in the graph. (D) Height and (E) amplitude images in solution. Particles indicated by green arrowheads in (D) were presumed to be MAS monomers. (F) Height distribution of MAS particles in solution based on measurements from six 1×1 μm solution images. Particles, with heights between 4.8 and 8.8 nm were considered to be MAS monomers. The average height obtained this way is 6.9 ± 1.1 nm. Unlike $rPrP^{C}$ (WT and 10OR) and BSA, some particles with smaller diameters had larger heights than particles with larger diameters in the same images. This characteristic made the standard deviation larger than those for 10OR and BSA. As a result, we used the combination of particle height and shape in amplitude images in order to more accurately determine the average size of presumed MAS monomers on mica.

To obtain these images, 5.6 μl of stock MAS (MW: ~224 KDa) solution (40 mg/ml MAS, 20 mM Tris, 50 mM NaCl, 2 mM DTT, 10 % Glycerol, pH 7.5) was mixed with 394.4 μl of PBS (1X, pH 7.4) to make 400 μl of about 2.5 μM MAS solution. To get the air images (A

and B), a 10 μl aliquot was deposited on freshly cleaved mica with subsequent Poly-L-lysine treatment for 4 minutes, rinsed with Milli-Q water and dried with compressed nitrogen gas (Poly-L-lysine treatment was used to change the negative charge of the mica surface into a positive charge due to the isoelectric point (4.93) of MAS. This treatment enabled us to attach MAS particles with a net negative charge at pH = 7.4 to the mica.). The sample was then imaged with tapping mode. To get the solution images (D and E), 45 μl aliquot was deposited on Poly-L-lysine treated mica secured to the AFM scanner and a fluid cell was installed. *In situ* imaging in taping mode was then carried out. Because MAS aggregation occurred easily during imaging process under the solution environment, only the first and second images taken after the quick initial engagement were used to get the average height of presumed MAS monomers. MAS imaging was repeated many times in order to increase the accuracy of the estimate of the presumed monomer height.

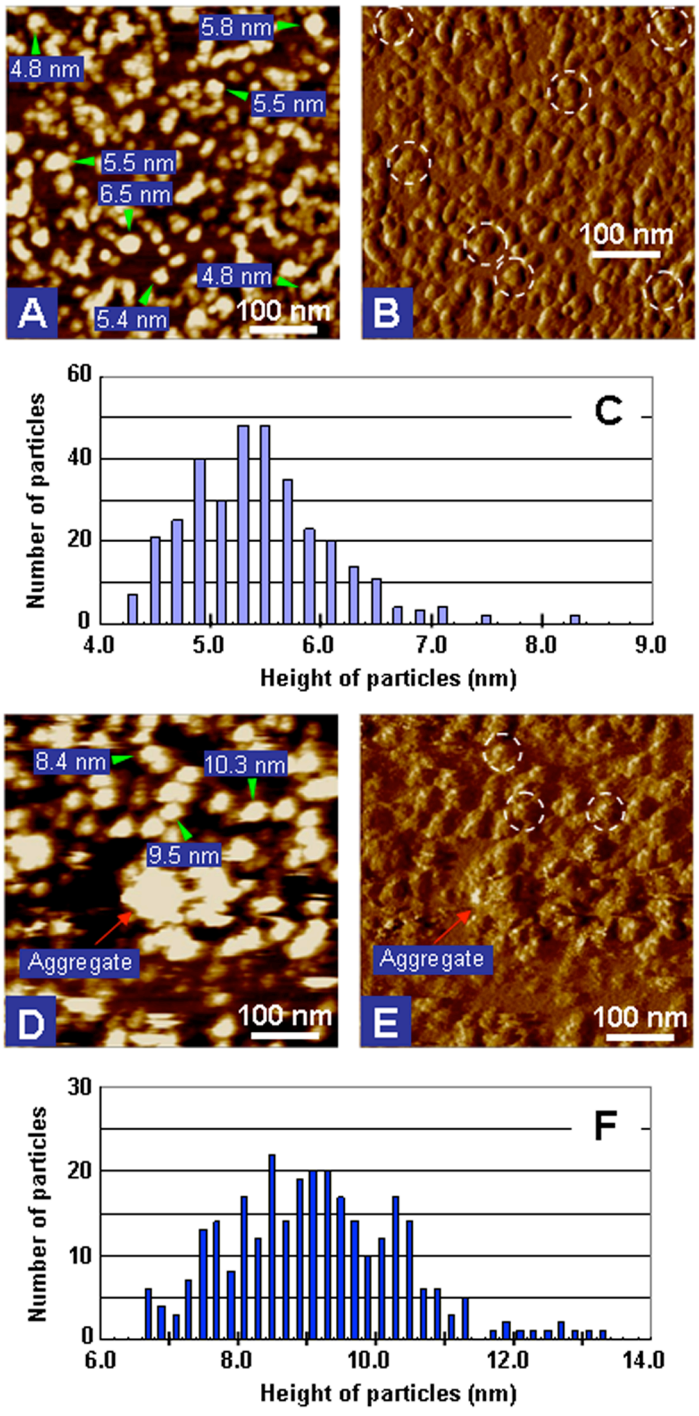

Figure S7. AFM images of Apoferritin from equine spleen (MW: ~481.2 KDa) and height

distributions.

(A) Height and (B) amplitude images collected in air. Particles are indicated by green arrowheads in (A) and circles in (B). (C) The height distribution of Apoferritin particles in air, based on measurements from six 500×500 nm air images. Particles, with heights between 4.2 and 6.6 nm, were used to estimate the average height of monomers. The average height obtained this way is 5.4 ± 0.54 nm. (D) Height and (E) amplitude images collected in solution. Particles indicated by green arrows in (D) and circles in (E) show typical Apoferritin monomers. (F) Height distribution of Apoferritin particles in solution based on measurements from six 500 × 500 nm solution images. Particles, with heights between 6.6 and 11.4 nm were used to get the average Apoferritin monomer height on mica in solution. The average height obtained this way is 9.0 ± 1.10 nm. Apoferritin aggregates like the one indicated by red arrows in (D) and (E), which are difficult to resolve into individual monomers were not used for the height measurements.

To obtain these images, 9.04 µl of Apoferritin (MW: ~481.2 KDa) solution (49 mg/ml, 0.15 M NaCl) from equine spleen (Sigma-Aldrich, A3641-100MG) was diluted into 490.96 µl of 20 mM NaOAc, pH 6.4 to make 500 µl of ~1.8 µM Apoferritin solution at pH 6.4. To get the air images (A and B), a 10 µl aliquot was deposited on freshly cleaved mica with subsequent Poly-L-lysine treatment for 4 minutes, rinsed with Milli-Q water and dried with compressed nitrogen

gas (Like previous MAS case, Poly-L-lysine treatment was used to change the negative charge of the mica surface into a positive charge due to the isoelectric point[5] (4.2-4.5) of Apoferritin from equine spleen. This treatment enabled us to attach Apoferritin particles with a net negative charge at pH = 6.4 to the mica effectively.). The sample was then imaged with tapping mode AFM. To get the solution images (D and E), 45 μl aliquot was deposited on Poly-L-lysine treated mica (diameter: 3 mm) secured to the AFM scanner and a fluid cell was installed. *In situ* imaging in tapping mode was then carried out.

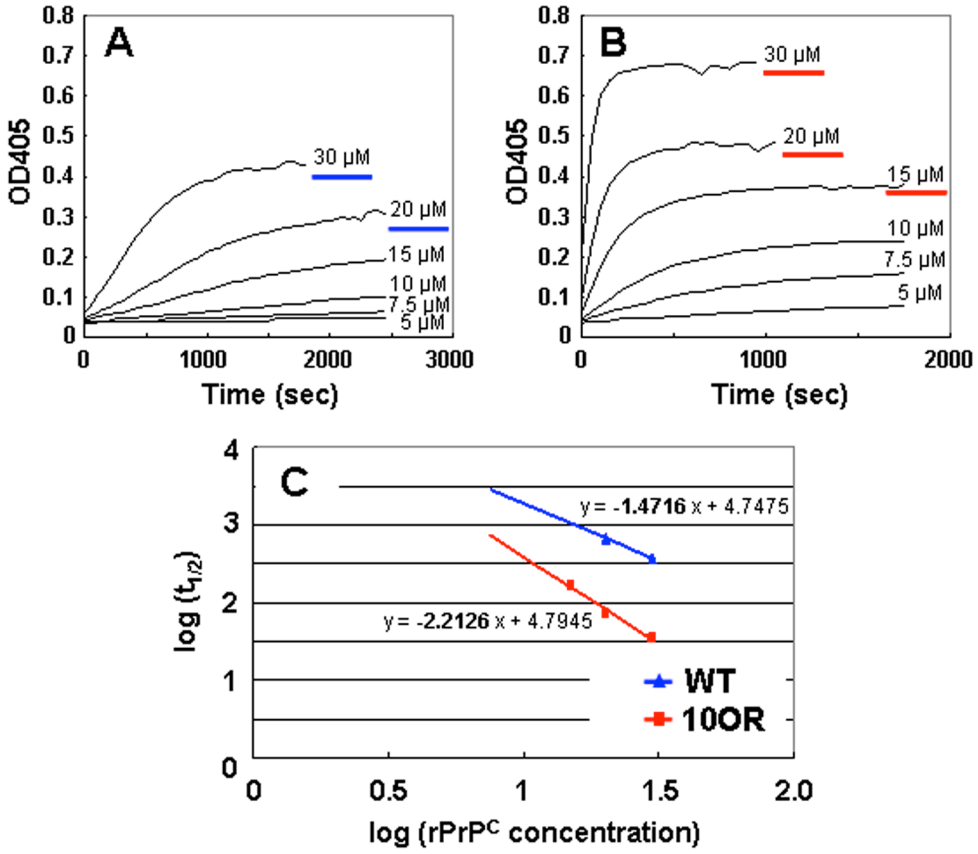

Figure S8. Turbidity assay and analysis of turbidity data to obtain an approximate seed size (the turbidity data were taken from ref 6).

(A) WT. (B) 10OR. (C) Plot of $t_{1/2}$ vs. rPrP^C concentration used to estimate seed size. The assay was performed at 37 °C in a volume of 200 µl in 96-well plates. A 100 µl solution of 1 M GdnHCl, 50 mM NaOAc, 150 mM NaCl (pH 4) was mixed with a 100 µl solution of rPrP^C (WT, 10OR) at various rPrP^C concentration suspended in 50 mM NaOAc, 150 mM NaCl (pH 4). Thus, final GdnHCl concentration in a 200 µl solution was 0.5 M and the final concentrations of rPrP^C

are shown above turbidity curves. Each solution was pre-incubated to 37 °C before mixing. After mixing, the turbidity of samples were monitored within 15 seconds by reading the attenuation at 405 nm in a Beckman Coulter AD340 micro-ELISA plate reader, using a kinetic photometric model (interval time: 50 seconds, 60 cycles with 1 second shaking before every cycle). For 20 μM $rPrP^C$, the time ($t_{1/2}$) to reach half-maximal signal was 680 seconds for WT and 75 seconds for 10OR when 15 seconds dead time was added. For 30 μM $rPrP^C$, $t_{1/2}$ was 375 seconds for WT and 35 seconds for 10OR. For 15 μM $rPrP^C$, 10OR reached the maximum signal and $t_{1/2}$ was 165 seconds, but WT did not reach the maximum signal within the time course of the test. The seed size is estimated by measuring the time to reach a certain extent of polymerization (i.e., the time it takes the monomer concentration to reach some arbitrary fraction of its initial value) as a function of protein concentration. Thus, in our case where we used $t_{1/2}$, two times the slope of log ($t_{1/2}$) versus log ($rPrP^C$ concentration) gives the seed size. WT indicates 2.9 and 10OR 4.4. Therefore, seed sizes for WT and 10OR are approximately considered as trimer or tetramer, in agreement with AFM data.

As we explain in the **Discussion** section of the paper on **Seed size**, this analysis to give an approximate seed size is applicable when the protein aggregation reaction satisfies "irreversibility" and "pre-equilibrium" conditions.[7] In addition, the analysis assumes that seeds form through one-by-one monomer attachment, but further growth of the seeds can occur either

by monomer or oligomer attachment. Irreversibility, which means that polymer production by the seed formation is irreversible, is well satisfied when the monomer concentration is much larger than the equilibrium monomer concentration (when the analysis is carried out in the kinetic regime of the protein aggregation). To satisfy the irreversibility condition, we used the time ($t_{1/2}$) taken to reach 50 % of maximum optical signal.

Pre-equilibrium means that polymers one monomer smaller than the seeds are in equilibrium with monomers throughout the aggregation reaction, i.e.,

$$(n-1)\alpha_1 = \alpha_{n-1}, \quad K = \frac{\alpha_{n-1}}{\alpha_1^{n-1}} \tag{1}$$

(n: seed, α_1: monomer concentration, α_{n-1}: concentration of polymers one monomer smaller than the seeds, K: equilibrium constant).

This pre-equilibrium condition is well satisfied when seed size is large rather than small and aggregation is relatively slow. This is because in these conditions, pre-seed aggregates easily repeat cycles of dissociation and growth many times before finally becoming seeds, thus keeping α_1 and α_{n-1} constant over time as aggregation proceeds.[7] This pre-equilibrium condition is applicable to rPrP aggregation in our current study even though seeds are small and aggregation is fast for the following reason.

In the cooperative polymerization model[7], the monomers are the species directly incorporating into the aggregate phase and, as explained in the **Discussion** section of the main

text on **Seed size**, in the current rPrP aggregation systems, these are the structure-altered monomers of concentration (α_1). When the partially denaturing acidic buffer is introduced into $rPrP^C$ solution, α-helix rich $rPrP^C$ monomers unfold and become the structure altered monomers that subsequently relax by forming seeds.

Unlike the situation in an aggregation system with a small seed where the monomer concentration typically decreases as aggregation proceeds, in the rPrP aggregation system structure altered monomers are continuously generated from the α-helix rich $rPrP^C$ monomers over some initial period. These structure altered monomers are consumed in forming dimers and seeds (the concentration of dimers, i.e., polymers one monomer smaller than the seed remains small because they easily develop into seeds). This may enable α_1 and α_{n-1} to be kept constant or nearly so over some period, thus satisfying the pre-equilibrium condition. As a result, the approximate rPrP seed size can be obtained by applying the above analytical method to the turbidity data. We note that our AFM and turbidity results together with those of a previous study[8] dealing with *in vitro* non-fibrillar aggregation of recombinant prion proteins suggest that, although the linear relationship between $\log\tau_D$ and $\log\alpha_0$ can give an approximate seed size when the system satisfies conditions of pre-equilibrium and irreversibility, it does not imply that further growth occurs by monomer attachment to the seeds.

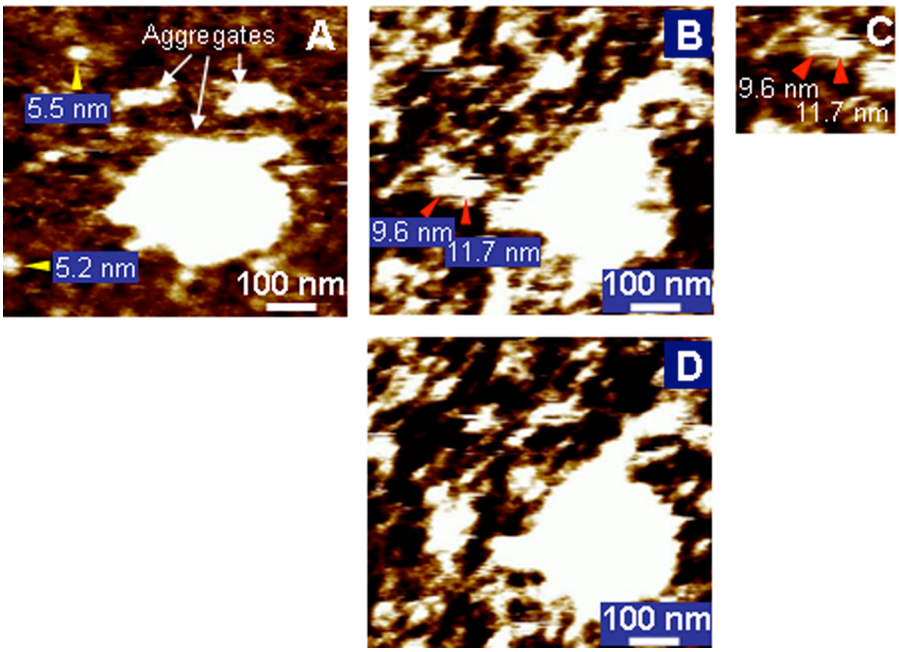

Figure S9. *In situ* (solution) AFM images showing aggregates and β-oligomers attaching to mica (Images (A) and (B) are Figure 4, H and I in the paper and (C) is a lower contrast image of the aggregate composed of two β-oligomers with heights 9.6 nm and 11.7 nm seen in (B)). To obtain these images, 50 µl of 20 µM 10OR suspended in 50 mM NaOAc, 150 mM NaCl (pH 4) and 50 µl of 1 M GdnHCl, 50 mM NaOAc, 150 mM NaCl (pH 4) were pre-incubated at 37 °C for 30 minutes and then mixed together to get 100 µl of 10 µM (final concentration) 10OR in 0.5 M (final concentration) GdnHCl, 50 mM NaOAc, 150 mM NaCl at pH = ~4. After mixing, followed by incubation for 5 minutes at room temperature, a 5 µl aliquot out of 100 µl was deposited on mica secured to the AFM scanner. 30 µl of pure buffer (50 mM NaOAc, 150 mM NaCl (pH 4)) was added to the 5 µl aliquot in order to dilute the protein concentration to lower

levels and thus slow down the reaction. The fluid cell was then installed and sealed to prevent evaporation. The AFM signal quickly stabilized and we were able to observe oligomer and aggregate growth phenomenon, which occurred primarily an incubation time of about 5 minutes at room temperature.

(A) Image at 57 minutes. Time was recorded just after the 5 µl aliquot was deposited on mica (57 minutes is the time when image capture was completed). The image shows small oligomers with heights of 5.2 nm and 5.5 nm interpreted to be trimers or tetramers according to the calibration curve of Figure 2 in the paper, and aggregates, which are seen to be composed of β-oligomers (by viewing them at lower contrast and using section analysis of the heights). At 93 minutes, 12 µl aliquot out of newly made 100 µl solution of 20 µM (final concentration) 10OR, 0.5 M (final concentration) GdnHCl, 50 mM NaOAc, 150 mM NaCl at pH = ~4, incubated for 2 minutes at room temperature using the same procedure described above, was injected into the fluid cell. When the signal had stabilized after the injection of this new solution, imaging again commenced. (B) Image at 122 minutes showing the same area where image (A) was captured. The subsequent images (B) and (C) show that more particles have formed, including a new aggregate composed of two β-oligomers with heights of 9.6 nm and 11.7 nm. (D) Image at 135 minutes showing the same area where images (A) and (B) were captured. The elapsed time between (B) and (D) is 13 minutes. The “peninsulas” that appear in (B) still remain in (D),

indicating the attachment of oligomers from newly prepared solution to the aggregates shown in (A) is permanent.

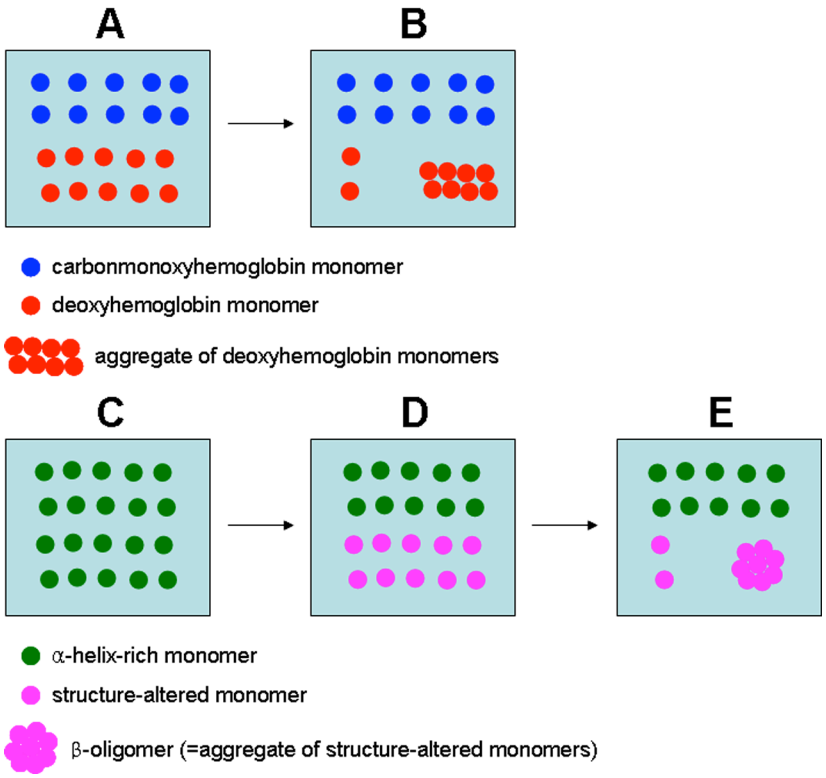

Figure S10. Schematic showing the similarity of the model for aggregation in the deoxyhemoglobin/carbonmonoxyhemoglobin system[9] and the rPrP α-helix-rich-monomer/structure-altered-monomer system.

(A) Initial state of the deoxyhemoglobin and carbonmonoxyhemoglobin solution at 1 °C before aggregation starts. The deoxyhemoglobin and carbonmonoxyhemoglobin exist as monomers. (B) Equilibrium state after the aggregation finished at 26 °C. Aggregates of deoxyhemoglobin monomers, deoxyhemoglobin monomers and carbonmonoxyhemoglobin monomers, which were almost completely excluded from the aggregates phase, coexist in equilibrium. (C) Initial state of

rPrP in 20 mM NaOAc, pH 5.5. It has α-helix rich structure and the majority remain as monomers. (D) Phenomenon occurring in rPrP solution as soon as the GdnHCl-containing acidic buffer is introduced into the rPrP solution. In analogy to the deoxyhemoglobin/carbonmonoxyhemoglobin system, the α-helix rich monomers and the structure-altered monomers play the role of the carbonmonoxyhemoglobin and deoxyhemoglobin, respectively. (E) Equilibrium state following formation of β-oligomers. The β-oligomers form by aggregation of the structure-altered monomers, which coexist in the solution with the α-helix rich monomers, the latter being excluded from the β-oligomers.

References

(1) Zahn, R. *J*. *Mol*. *Biol*. **2003**, *334*, 477-488.

(2) Maiti, N. R.; Surewicz, W. K. *J*. *Biol*. *Chem*. **2001**, *276*, 2427-2431.

(3) Bae, S.-H.; Legname, G.; Serban, A.; Prusiner, S. B.; Wright, P. E.; Dyson, H. J. *Biochemistry* **2009**, *48*, 8120-8128.

(4) Thirumalai, D.; Klimov, D. K.; Dima, R. I. *Curr. Opin. Struct. Biol.* **2003**, *13*, 146-159.

(5) Wittig, I.; Karas, M.; Schägger, H. *Mol. Cell. Proteomics* **2007**, *6*, 1215-1225.

(6) Yu, S.; Yin, S.; Li, C.; Wong, P.; Chang, B.; Xiao, F.; Kang, S. –C.; Yan, H.; Xiao, G.; Tien, P.; Sy, M. –S. *Biochem*. *J*. **2007**, *403*, 343-351.

(7) Goldstein, R. F.; Stryer, L. *Biophys*. *J*. **1986**, *50*, 583-599.

(8) Frankenfield, K. N.; Powers, E. T.; Kelly, J. W. *Protein*. *Sci*. **2005**, *14*, 2154-2166.

(9) Hofrichter, J.; Ross, P. D.; Eaton, W. A. *Proc*. *Natl*. *Acad*. *Sci*. *U.S.A*. **1976**, *73*, 3035-3039.

Full citation for Reference 2 from Main Text:

Maraganore, D. M.; de Andrade, M.; Elbaz, A.; Farrer, M. J.; Ioannidis, J. P.; Krüger, R.; Rocca, W. A.; Schneider, N. K.; Lesnick, T. G.; Lincoln, S. J.; Hulihan, M. M.; Aasly, J. O.; Ashizawa, T.; Chartier-Harlin, M. –C.; Checkoway, H.; Ferrarese, C.; Hadjigeorgiou, G.; Hattori, N.; Kawakami, H.; Lambert, J. –C.; Lynch, T.; Mellick, G. D.; Papapetropoulos, S.; Parsian, A.;

Quattrone, A.; Riess, O.; Tan, E. –K.; Van Broeckhoven, C. *J*. *Am*. *Med*. *Assoc*. **2006**, *296*, 661-670.